Temporal dynamics of leaf area index and land surface temperature correlation using Sentinel-2 and Landsat OLI data

Ali Yasin Ahmed[1*] , Abebe Mohammed Ali[2] and Nurhussen Ahmed[2]

Abstract

Background Understanding the complex relationship between vegetation dynamics and land surface temperature (LST) is crucial for comprehending ecosystem functioning, climate change impacts, and sustainable land management. Hence, this study conducts a temporal analysis of leaf area index (LAI) and LST data derived from Sentinel-2 and Landsat Operational Land Imagery (OLI) in the Mille River Basin, a tropical region in Ethiopia. LAI data were generated using Sentinel-2 imagery processed with the Sentinel Application Platform (SNAP) toolbox, an open-access earth observation analysis tool, while Landsat OLI collection 2 level 2 data were utilized for precise LST retrieval. The Mann–Kendall test was used to detect trends in the time series data.

Results The trends in the mean LAI were statistically significant at P values of 0.05 and 0.10 for the annual and seasonal trends, respectively. The mean LST trends were insignificant throughout the study period except for the summer season, for which the P value was 0.07. The correlation between the LAI and LST was weak ($R^2 = 0.36$) during the crop-growing seasons (summer and spring) but moderate in winter ($R^2 = 0.46$) and autumn ($R^2 = 0.41$).

Conclusion The findings of this research clarify the complex relationships between variations in surface temperature and vegetation growth patterns, providing insight into the environmental mechanisms driving the dynamics of localized ecosystems. The study underscores the implications of these findings for informed decision-making in sustainable land management, biodiversity conservation, and climate change mitigation strategies.

Keywords Leaf area index, Land surface temperature, Land use management, Vegetation dynamics, Remote sensing

Background

Understanding the dynamics of vegetation and land surface temperature (LST) has paramount implications for ecological and climate change assessments and land resource management studies. The leaf area index (LAI), a critical biophysical variable measuring the total area of leaves relative to the land surface, plays a critical role in comprehending land surface processes associated with vegetation dynamics and climate modeling (Avdan and Jovanovska 2016; Mwangi et al. 2018). This approach provides essential insights into the impacts of various environmental factors on vegetation (Wang et al. 2019). Similarly, LST, another significant variable linked to vegetation dynamics, is directly influenced by vegetation conditions (Guechi et al. 2021; Zhao-Liang et al. 2013).

A comprehensive global vegetation analysis spanning 31 years (1982–2013) across all continents revealed a persistent browning trend on Earth since the 1990s (Pan et al. 2018). Nonetheless, other studies have indicated a contrasting greening trend, primarily driven by human land-use practices. For example, Park et al. (2019) demonstrated substantial contributions to the greening trend

*Correspondence:
Ali Yasin Ahmed
alexoy5050@gmail.com
[1] Department of Geography and Environmental Studies, Jigjiga University, P.O. Box 1020, Jigjiga, Ethiopia
[2] Department of Geography and Environmental Studies, Wollo University, P.O. Box 1145, Dessie, Ethiopia

Ahmed *et al. Environmental Systems Research*   (2024) 13:43

Page 2 of 15

in China and India, with China accounting for 25% of the global increase in leaf area and India exhibiting an increase exceeding 35% since 2000. The ongoing browning trend in global vegetation since the 1990s emphasizes the impact of climate on vegetation. However, the concurrent greening trend, exemplified by significant leaf area increases in China and India, suggests that human land-use practices significantly influence vegetation (Pan et al. 2018).

The relationship between vegetation and LST has been extensively studied and established as an inverse relationship (Hussain et al. 2023; Jin and Zhang 2002; Mwangi et al. 2018; Rasul et al. 2020). This inverse relationship is driven by several physiological and physical mechanisms. Several researchers have agreed on this inverse relationship, attributing it to the cooling effect of vegetation on the land surface, where an increase in the number of plants corresponds to a decrease in LST (Nega et al. 2019). This cooling effect arises from the transpiration of water by plants, which regulates the temperature of the surrounding environment (Schwaab et al. 2021). Additionally, this relationship is influenced by factors such as solar radiation, atmospheric conditions, and soil moisture (Liu et al. 2016). Furthermore, the vegetation canopy itself absorbs more energy, which is utilized in photosynthesis and other metabolic processes rather than being converted into heat (Baldocchi et al. 2002; Kume 2017). This absorption, coupled with the cooling effect of transpiration, significantly moderates the local temperature. Generally, heightened solar radiation and reduced atmospheric moisture levels tend to elevate LSTs (Cheruy et al. 2017; Han et al. 2020; Jiang et al. 2023), whereas increased vegetation and soil moisture assist in lowering LSTs (Imran et al. 2021; Li et al. 2022; Liu et al. 2016).

Previous studies have utilized various satellite datasets, such as MODIS, to investigate the connection between the LAI and LST (Hussain et al. 2023; Miller et al. 2022; Mwangi et al. 2018; Rasul et al. 2020; Reygadas et al. 2020; Schwaab et al. 2021; Tesemma et al. 2015). Despite the growing importance of remote sensing data in environmental monitoring and land management (Woodcock et al. 1983; Skidmore 2002; Skidmore et al. 1997), there is still a critical gap in the understanding of the temporal dynamics and interrelationship between LAI and LST, as derived from Sentinel-2 and Landsat Operational Land Imager (OLI) data. Sentinel-2 and Landsat OLI offer higher spatial resolution compared to MODIS, with Sentinel-2 providing 10–60 m and Landsat OLI 30-m resolution, whereas MODIS offers a coarser resolution of 250–1000 m. While the broader resolution, daily revisit time, and higher spectral capabilities make MODIS an excellent data source for frequent and large-scale monitoring (Myneni 1997; Reygadas et al. 2020), Sentinel-2

and Landsat OLI offer finer spatial detail that enhances the accuracy and applicability of LAI and LST measurements for more localized studies. However, the combined analysis and temporal association of these metrics using time-series data from these two prominent satellite platforms have been relatively underexplored.

Ethiopia, located in the Horn of Africa, is renowned for its diverse climatic zones and rich biodiversity (Fashing et al. 2022), making it an ideal study area for examining the dynamics between LAI and LST. The country's topography ranges from lowland to highland plateaus, contributing to varied climatic conditions that influence vegetation patterns (Birhanu et al. 2021). Despite this ecological importance, there has been a notable lack of research specifically addressing the relationship and trends between LAI and LST in Ethiopia. Most studies conducted in the country have concentrated on vegetation dynamics using vegetation indices (Muir et al. 2021; Seneshaw Getahun 2015; Worku et al. 2023) or examined the impact of land use and land cover (LULC) changes on LST (Haylemariyam 2018; Moisa et al. 2022a, b; Yeneneh et al. 2022). These studies have provided valuable insights into the overall health and distribution of vegetation, as well as how land cover changes affect surface temperatures. However, the specific interactions between LAI and LST are still not well understood.

This research aims to bridge these gaps by conducting a meticulous time series analysis of LAI and LST data derived from Sentinel-2 and Landsat OLI data in the Mille River Basin, a tropical region in Ethiopia. By exploring the intricate connections between changes in LAI and LST, our research aims to offer a valuable understanding of the fundamental ecological mechanisms at play and their significance for promoting sustainable land management techniques and strategies for mitigating the effects of climate change. Through this integrated approach, we aim to contribute to the refinement of remote sensing methodologies and the advancement of our understanding of local-scale environmental dynamics.

The findings of this study highlight the significance of employing high-resolution satellite imagery to examine the connection between vegetation status and climate at a local scale, particularly in areas characterized by diverse landscape features that can impact the association between LAI and LST. It offers a comprehensive evaluation of these relationships and emphasizes the potential of high-resolution satellite imagery for understanding the complex interactions between vegetation and climate. The results contribute to the existing knowledge of this association and provide valuable insights into its potential consequences for vegetation dynamics and climate modeling at the local scale. Thus, this research has two main objectives: (a) assessing the time-series trends

of the mean LAI and LST derived from Sentinel-2 and Landsat OLI data and (b) evaluating the seasonal and annual correlations between these two variables.

Materials and methods

Description of the study area

The study was conducted in the lower Millie watershed, situated in Ambasel District within the South Wollo Zone of the Amhara Regional State, Ethiopia (Fig. 1). The area encompasses both tropical and subtropical agroclimatic regions. Millie watershed is positioned between 11.32^0 and 11.54^0 latitude and 39.52^0 and 39.68^0 longitude. The study area encompasses approximately 19,509 hectares. The elevation within this region varies from 1,427 to 3,635 m above sea level, indicating the presence of multiple agroclimatic zones. In addition, the region exhibits an average temperature varying between 15 and 20 °C (Destaw 2017). The data obtained from the Kombelcha meteorological station suggest that the study area experiences annual precipitation ranging from 800 to 1200 mm.

The primary rainy season typically spans from June to August, while short rains characterize the period between April and June. The region experiences its lowest minimum temperatures from August to November, ranging from 11 to 12 °C. Conversely, the highest maximum temperatures occur during May and June, varying between 22 and 30 °C. The livelihood of the study area is largely reliant on agriculture which is predominantly influenced by rainfall. The predominant vegetation in the study area includes Eucalyptus trees and various perennial fruiting plants (Desalegn et al. 2023). Agriculture serves as the dominant occupation, engaging a significant portion of the population.

Data processing

Sentinel-2 data and preprocessing

The estimation of LAI utilizing the Sentinel Application Platform (SNAP) toolbox involved the use of Sentinel-2 satellite images. Specifically, the dataset comprises more than 36 cloud-free Level 1C from 2016 to 2018 and Level 2A images from 2019 to 2022. The Level 2A images, accessible free of charge from the Copernicus SciHub website (https://scihub.copernicus.eu/), are both geometrically and atmospherically corrected, providing a bottom-of-atmosphere (BOA)-corrected reflectance product (Wang et al. 2019). However, preprocessing is required for Level 1C images before biophysical retrieval (Sola et al. 2018).

Sentinel-2 Level 2A data is preferred over Level 1C primarily because it provides surface reflectance values corrected for atmospheric conditions, enhancing the accuracy of the derived vegetation indices or biophysical variables (Moravec et al. 2021). This correction minimizes atmospheric effects, such as aerosols and water vapor, which can distort the true surface reflectance. Additionally, this data includes quality indicators that help in identifying and excluding clouds and shadows, further improving the reliability of our analysis. To convert the Level 1C data to Level 2A data, the Sen2Cor atmospheric
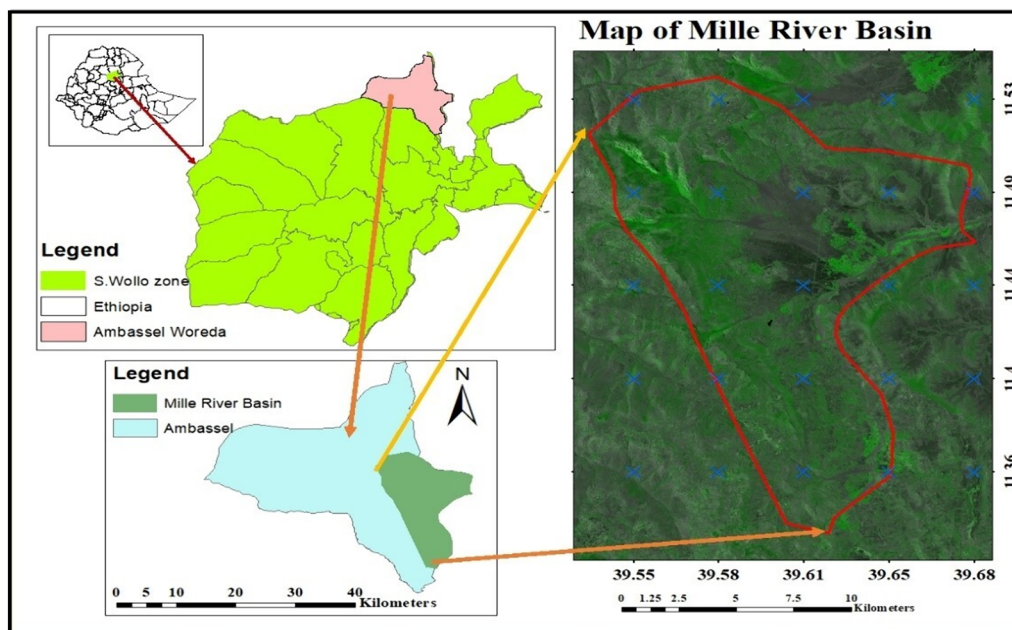

Fig. 1 Map of the Millie watershed, which displays a true color combination of the Sentinel-2 satellite images (bands 4, 3, and 2)

correction algorithm was employed, a method demonstrated in the work of Kganyago et al. (2020). This algorithm effectively addresses atmospheric distortions in Level-1C data, producing BOA reflectance images with the option of terrain and cirrus correction (Clevers et al. 2017).

Standardizing the analysis, all the atmospherically corrected images were resampled to a 20-m pixel size, ensuring uniformity across all the available bands of the Sentinel-2 images. Within the SNAP toolbox, three biophysical processors were available, namely, S2_20m, S2_10m, and LANDSAT8 (Mourad et al. 2020). For this particular study, the S2_20m processor was utilized to estimate the LAI of the study area. To assess the LAI trend from 2016 to 2022, a total of 36 Sentinel-2 images were employed.

The images were acquired with no more than a 10-day difference between Sentinel-2 and Landsat, ensuring consistency throughout all acquisition periods. Table 1 provides an overview of the data sources used for LST and LAI retrieval, including acquisition dates, resolution, and specific bands or levels used for each dataset.

Landsat level 2 LST product and preprocessing

In our study, we used the Landsat Collection 2 Level 2 data, which provides a pre-calculated LST product. The Landsat 8–9 Collection 2 Level 2 LST data were computed using the single channel method from the Landsat 8–9 Collection 2 Level 1 Thermal Infrared Sensor (TIRS) Band 10 using the Top of Atmosphere (TOA) Reflectance, TOA Brightness Temperature (BT), Advanced Space borne Thermal Emission and Reflection Radiometer (ASTER), Global Emissivity Dataset (GED) data, ASTER Normalized Difference Vegetation Index (NDVI) data, and atmospheric profiles of geopotential height, specific humidity, and air temperature extracted from reanalysis data (Sayler 2022). In the Collection 2 Level 2 dataset for Landsat 8/9, LST is derived using the single-channel method with thermal Band 10, while Band 11, which is also a thermal band, is excluded from the LST calculation. TOA Reflectance refers to the reflectance of solar radiation from the Earth's surface as measured at the satellite sensor (Sharma et al. 2009). It represents the fraction of incoming solar radiation that is reflected by the Earth's surface and atmosphere combined. TOA BT is the temperature of a blackbody that emits the same amount of radiation as measured by the satellite sensor at the top of the atmosphere (Wang and Gastellu-Etchegorry 2020). It is derived from the thermal infrared bands of the Landsat imagery. GED provides emissivity values for different land cover types, which can be applied to the TOA BT to derive the true LST (Mustafa et al. 2020).

The digital number (DN) values are then transformed to LST using a multiplication factor (0.00341802) and an additive number (149), as shown in Eq. 1 (Sayler et al. 2023). The value 149 is an empirically derived constant that adjusts the scaled DN values into the correct temperature range for Band 10 (Sayler 2022). The output unit for the LST is in Kelvin, which is converted to Celsius by subtracting 273.15. Its accuracy is validated with an R^2 of 0.997 by Crawford et al. (2023) and an R^2 of 0.96 by Wachmann et al. (2024). To ensure consistency with the LAI pixel size, the LST data were resampled to a 20-m pixel size and reprojected to UTM zone 37N.

$$LST = (DN * 0.00341802 + 149) - 273.15 \quad (1)$$

Cloud-free Landsat imagery was obtained from NASA's website, comprising Level 2 Landsat 8 and 9 OLI, to estimate the LST of the Millie watershed from 2016 to 2022. We used over 40 collection 2 Level 2 Landsat images spanning 7 consecutive years, with multiple images collected for each season, particularly during the rainy seasons (spring and summer). To address cloud cover, we replaced cloudy pixels with data from clear-sky images. This approach allowed us to create cloud-free images by combining multiple observations over time. The Landsat satellite data have a spatial resolution of 30 m, and the imagery can be downloaded free of charge from the USGS Earth Explorer (https://earthexplorer.usgs.gov/).

Table 1 Summary of data sources for LST and LAI retrievals

Data source	Date of acquisition	Spatial resolution	Level	Description
Landsat 8/9	2016–2022	30	Level 2	LST retrieval
Sentinel-2	2016–2018	10, 20, 60	Level 1C	Pre-processed imagery, LAI retrieval
Sentinel-2	2019–2022	10, 20, 60	Level 2A	LAI retrieval (atmospherically corrected)

Ahmed *et al. Environmental Systems Research*   (2024) 13:43

Page 5 of 15

LAI retrieval

The biophysical variable retrieval algorithm of the SNAP Toolbox for Sentinel-2, as described by Weiss and Baret (2016), is built on the PROSAIL radiative transfer model for canopy architecture and the artificial neural network (ANN) algorithm. The PROSAIL model is a widely used radiative transfer model that combines the PROSPECT leaf optical properties model and the SAIL canopy bidirectional reflectance model (Berger et al. 2018; Jacquemoud et al. 2009). The PROSPECT model simulates the optical properties of leaves based on their biochemical composition, including pigments, water content, and dry matter (Jacquemoud et al. 1996; Jiang et al. 2018). The SAIL (Scattering by Arbitrarily Inclined Leaves) model simulates the reflectance of the entire canopy by considering factors such as leaf area index (LAI), leaf angle distribution, and soil background (Han et al. 2023). Together, PROSAIL allows for the accurate simulation of vegetation reflectance across various wavelengths, making it a valuable tool in remote sensing for estimating vegetation properties and monitoring plant health.

Leveraging instant top-of-canopy reflectance data from eight Sentinel-2 bands, along with viewing zenith, solar zenith, and relative azimuth angles, the SNAP biophysical processor parameterizes PROSAIL to simulate bottom-of-atmosphere reflectance (Xie et al. 2019). Subsequently, the ANN algorithm, trained on the simulated reflectance, is applied to the chosen Sentinel-2 bands to retrieve the biophysical variable, as explained by Weiss and Baret (2016). This algorithm is categorized as "nonspecific," indicating its ability to deliver reasonable biophysical variable performance for various types of vegetation (Kamenova and Dimitrov 2021; Kganyago et al. 2020; Mourad et al. 2020; Xie et al. 2019). For reference, Table 2 outlines the bands required for LAI estimation using the SNAP toolbox.

The accuracy of the leaf area index (LAI) derived from the SNAP toolbox was evaluated to ascertain its reliability in practical applications. The study findings revealed a strong correlation ($R^2 = 0.74$) between the LAI values obtained through the SNAP toolbox and those acquired through direct field measurements. Figure 2 visually depicts the validation results, illustrating the consistency and coherence between the estimated and ground-measured LAI values. A root mean square error (RMSE) of 0.53 indicated an acceptable deviation between the SNAP-derived and actual field-measured LAI values, emphasizing the tool's ability to provide reliable estimates. Although suggesting a slight overestimation, the calculated bias of 0.31 was within an acceptable range, reinforcing the credibility of the SNAP toolbox-derived LAI values. Overall, the strong correlation, low RMSE, and minimal bias collectively underscored the reliability and accuracy of the SNAP toolbox-derived LAI values, affirming its practical utility in estimating and predicting the leaf area index in the study area. These findings contribute to the validation and endorsement of the effectiveness of the SNAP toolbox in generating accurate LAI data for further time-series analysis.

Trends and correlation analyses

In this study, local-scale changes in the LAI and LST and their interconnections were assessed using trend and regression analyses. MATLAB R2020a and R 4.0.3 software were used for all the statistical analyses.

Trend analysis

The trend analysis for both annual and seasonal trends relied on the SNAP-derived LAI and Landsat Level 2 LST products. Estimations of annual and seasonal trends were conducted using Zhang's method and the Yue Pilon method found in the "zyp" package within R software (Wang and Swail 2001; Yue et al. 2002). This approach is advantageous because of its accurate confidence intervals and robustness against outliers. Moreover, the widely
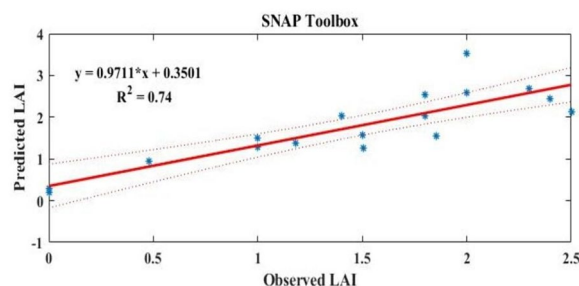
Table 2 Sentinel-2 spectral and spatial characteristics of the 8 selected bands

Band number	Central WL (nm)	Width (nm)	Spatial resolution (m)
Band 3	560	35	10
Band 4	665	30	10
Band 5	705	15	20
Band 6	740	15	20
Band 7	783	20	20
Band 8a	865	20	20
Band 11	1610	90	20
Band 12	2190	180	20

Fig. 2 Validation of the SNAP toolbox and MVLR model-derived LAI using ground-measured LAI data

Ahmed *et al. Environmental Systems Research* (2024) 13:43

Page 6 of 15

recognized Mann–Kendall test was used to detect trends in time series data, as commonly observed in environmental studies, hydrology, and climatology (Hamed 2008). The Mann–Kendall test allows for the assessment of monotonic trends in data, where a significant test statistic leads to the rejection of the null hypothesis (Yue and Wang 2004).

While the Mann–Kendall test is effective at handling tied observations and outliers (Wang et al. 2020), it has limitations, such as its inability to detect nonlinear trends or abrupt changes in trend direction (Blain 2013). To mitigate these limitations, Sen's slope estimator and the Theil–Sen estimator were combined with the Mann–Kendall test, providing a comprehensive analysis of trend behavior. Additionally, given the requirement of non-autocorrelated data, the data were tested in R Studio using the plot method of autocorrelation using the ACF function. Equation 2 was used in the Mann–Kendall test for the analysis of the time series.

$$S = \sum_{i=1}^{n-1} \sum_{j=k+1}^{n} sign\,(xj - xi) \qquad (2)$$

Let X1, X2, and Xn represent the variables denoting n points of LAI and LST. The Mann–Kendall test (S) was then applied to these variables.

The Mann–Kendall test furnishes insights into the trend direction, if any, within the time series. A negative test result implies a decrease in both the LAI and LST, while a positive value suggests an increase. Conversely, a result of zero supports the null hypothesis of no trend. A positive S value suggests that the later observations in the series are expected to be greater than the earlier ones, while a negative S value suggests the opposite. The variance in S is calculated using Eq. 3.

$$Var = \frac{1}{18}\left[n\,(n-1)(2n+5) - \sum_{t} ft\,(ft-1)(2ft+5)\right] \quad (3)$$

In the Mann–Kendall test, the test statistic (Eq. 4) accounts for the variation in "t" across the set of tied ranks and the frequency "ft" at which the rank "t" appears. The test statistic is calculated using the following equation:

$$Z = \begin{cases} (S-1)\big/ & se, & S > 0 \\ & 0 & S = 0 \\ S + 1\big/ & se & S < 0 \end{cases} \qquad (4)$$

Here, *se* represents the square root of the variance.

Association analysis
The relationship between LAI and LST was assessed using a linear regression model, with the strength of the association quantified by the R-squared (R^2) value, calculated using Eq. 5. The significance level was set at $\alpha = 0.01$. To address potential discrepancies in data scales between the Sentinel-2 and Landsat OLI datasets, we implemented several preprocessing steps, including resampling to a uniform pixel size, reprojection to a common coordinate system, and temporal alignment by selecting images captured as close in time as possible.

$$R^2 = 1 - \frac{\sum (yi - y')^2}{\sum (yi - y')^2} \qquad (5)$$

Results
Seasonal and annual trends in the LAI and LST (2016–2022)
Seasonal trend of mean LAI
Figure 3 presents the mean LAI maps for each year of the study period from 2016 to 2022, illustrating spatial variations in vegetation density across the study area. Throughout the study period (2016–2022), all the seasons exhibited significant greening trends, with the exception of the spring season, which had a Sen slope of −0.041. The rate of change in the LAI demonstrated significant variation, ranging from 0.02 to 0.08 for the season-to-season trend and from 0.13 to 0.57 over the study period (trendP).

Figure 4 shows the seasonal trends and the trendP determined for each season from the Sentinel-2 images. Particularly, the autumn season demonstrated the highest trend (0.082) and trendP (0.576) with a Sen slope of 0.15. In general, the average LAI for all the seasons exhibited a notable greening trend over the study period. Table 3 highlights the seasons with a statistically significant trend at a p value of 0.05 in bold font.

Annual trend of mean LAI from 2016 to 2022
The annual trend in the mean LAI for the study area is depicted in Fig. 5. The analysis revealed a substantial greening trend, represented by a Sen's slope of 0.084 and a P value of 0.05 for the study period. The year-to-year trend in the mean LAI was 0.013, and the trend for the entire period was 0.091. The highest mean annual LAI in the study area was observed in 2021.

Seasonal trend of mean LST
The trends in LST for the four seasons are shown in Fig. 6. Variations in the trend and trendp of the LST were observed across seasons. However, the study did not identify any statistically significant seasonal trend in the mean LST during the study period (2016–2022), except for the summer season, which exhibited a seasonal trend in the LST with a P value of 0.07.
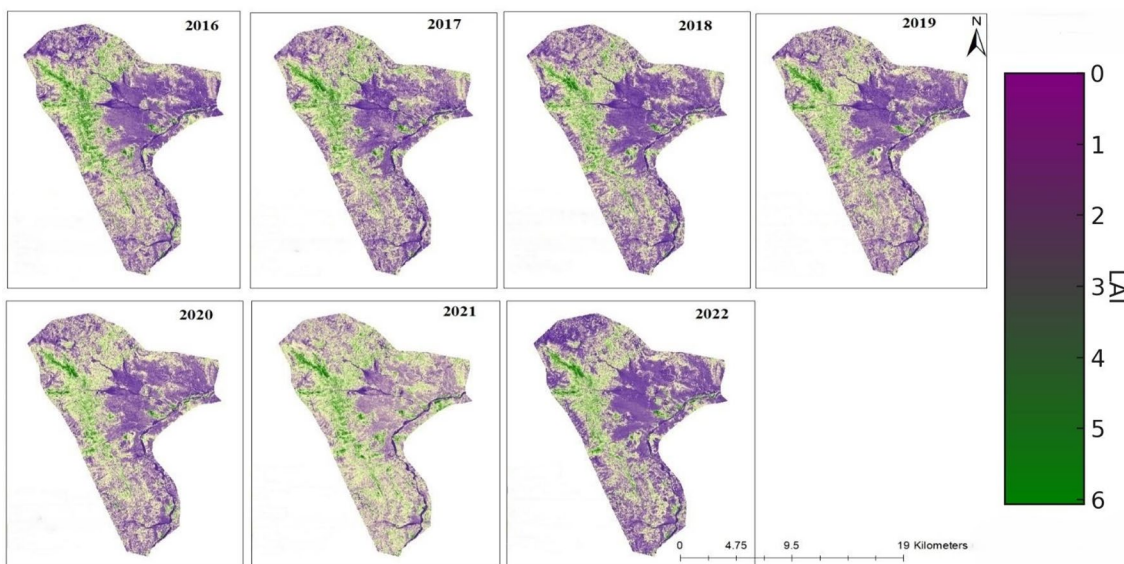
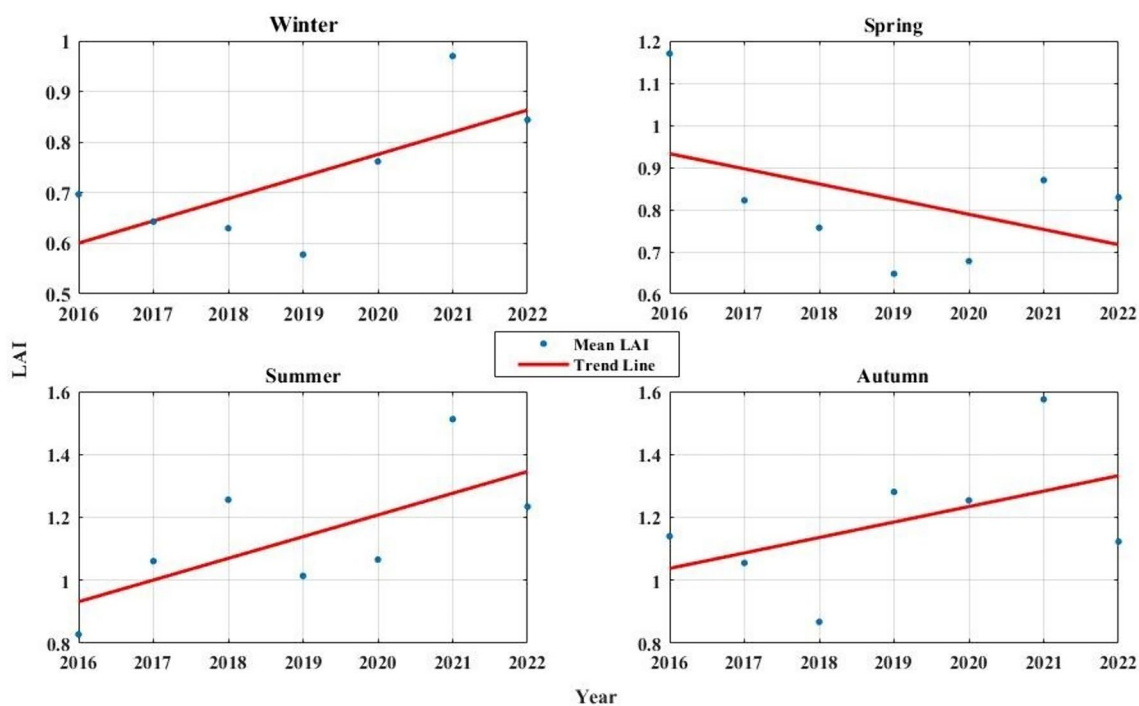**Fig. 3** Mean annual LAI maps of the study area from 2016 to 2022

Fig. 4 Seasonal Trends of LAI from 2016 to 2022. Sen's slope indicates the direction of LAI trends during the study period. All seasons showed a positive trend, except for spring, which had a Sen slope value of -0.041

During the spring season, a nearly zero trend (trend = 0.1) was observed, while increasing trends were noted in the summer seasons of 2021 and 2022. The season-to-season trend in the mean LST ranged from -0.031 (autumn season) to 1.5 (summer season), while for the trend period, it varied from -2.147 (autumn season) to 10.5 (summer season). Table 4 presents the statistical results of the mean LST trends for each season alongside the annual mean LST trend.

Table 3 Z values, Sen's slopes, P values, trends, and trends of the seasonal and annual trends of LAI from 2016 to 2022

Seasons	Z value	Sen's Slope	P value	Trend	TrendP
Winter	1.503	0.055	0.13	0.066	0.464
Spring	1.503	-0.041	0.13	0.020	0.137
Summer	1.503	0.052	0.13	0.052	0.364
Autumn	**1.878**	**0.047**	**0.05**	**0.082**	**0.576**
Annual	**1.878**	**0.013**	**0.05**	**0.013**	**0.091**

Annual trend of mean LST from 2016 to 2022

The annual trend in the mean LST for the study area was assessed based on the mean annual LST values over the study period. To ascertain the significance of the observed changes, the Mann–Kendall trend test was conducted, for which the P value was 0.1. Figure 7 displays the average LST maps for each year of the study period from 2016 to 2022, highlighting spatial variations in surface temperature across the study area.

The study findings indicated the absence of a significant annual trend in the mean LST. The year-to-year trend in the LST was 0.466, while for the trend period, it was 3.260 (Fig. 8). The highest mean annual LST in the study area was observed in 2021, which coincided with the year in which the highest mean LAI was recorded during the study period. Overall, the average annual LST did not significantly change over the study period, with a P value of 0.2.

Correlation
Annual relationship between LST and LAI
The assessment of the association between the LAI and LST was conducted at both annual and seasonal scales. To facilitate this analysis, all the LAI and LST seasonal images for each year were stacked and averaged using cell statistics (Fig. 9a, b). Similarly, for the seasonal analysis,
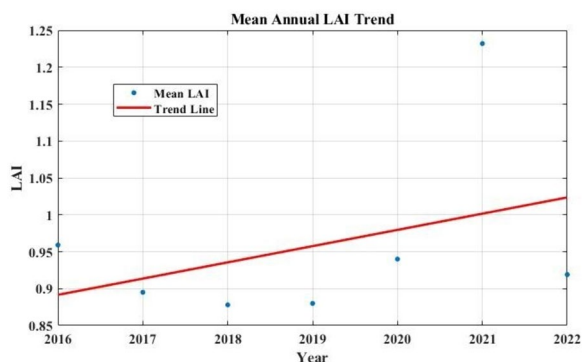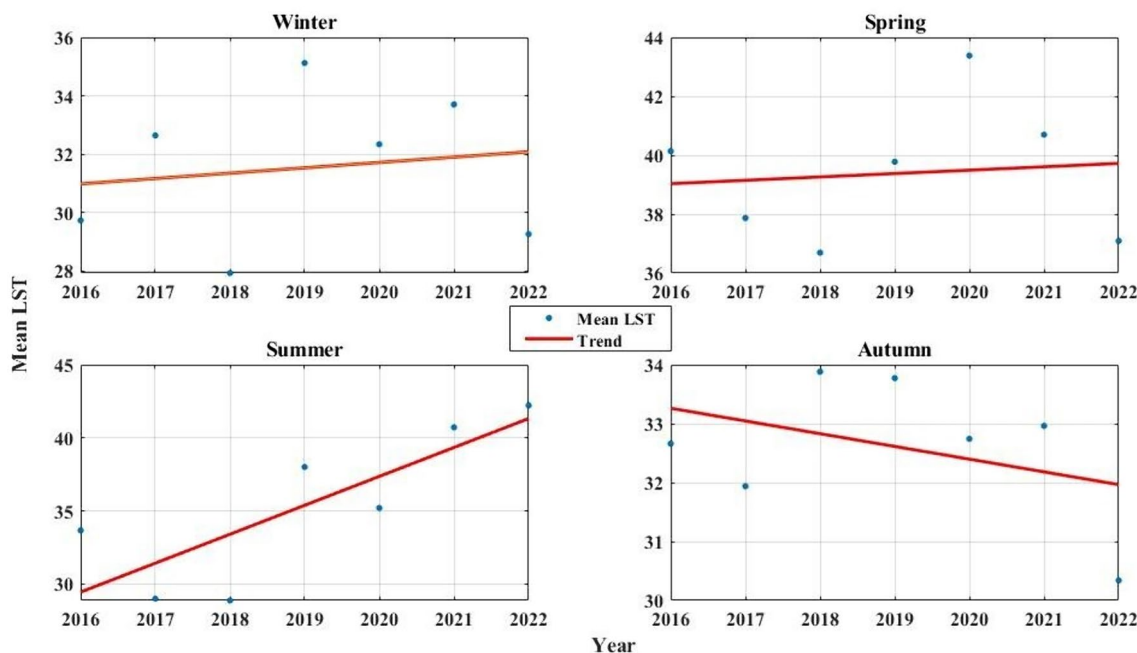

Fig. 5 Annual trend of mean LAI from 2016 to 2022: a positive trend with a 0.084 Sen's slope and a 0.05 P value

Fig. 6 Seasonal trends of mean LST from 2016 to 2022; Sen's slope shows the trend direction of the LST during the study period. All the seasons had insignificant positive and negative trends except for the summer season, which had a P value of 0.07

Ahmed *et al. Environmental Systems Research*   (2024) 13:43

Page 9 of 15

Table 4 Z values, Sen's slopes, P values, trends, and trends of the seasonal and annual trends of LST from 2016 to 2022

Seasons	Z value	Sen's Slope	P value	Trend	Trendp
Winter	0.00	0.265	1	0.265	1.853
Spring	0.00	0.10	1	0.100	0.700
Summer	1.802	1.5	0.07	1.500	10.500
Autumn	−0.30	−0.307	0.7	−0.307	−2.147
Annual	1.201	0.466	0.2	0.466	3.260

LAI and LST images for the same season across the seven years were stacked and averaged accordingly.

A total of 201 points were used to evaluate the association between the LAI and LST at both scales. The two variables exhibited a moderate correlation, with R-squared (R^2) values ranging from 0.35 to 0.49. This indicates that the vegetation characteristics of the study area respond to changes in LST. Particularly, the lowest R^2 value of 0.35 was recorded in 2021, while the highest value was observed in 2020 ($R^2 = 0.49$).

Seasonal relationship between the LAI and LST

The study area exhibited significant spatial and temporal variations in the distributions of LAI and LST. Consequently, the seasonal association between the LAI and LST was evaluated to discern the influence of LST on the LAI across the winter, spring, summer, and autumn seasons. The results of the linear regression model fitting between LAI and LST are depicted in Fig. 10.

The highest correlation between the LAI and LST was observed during the winter season ($R^2 = 0.46$), while the lowest R^2 value of 0.36 was recorded during the spring season. Overall, the correlation between LST and LAI across all seasons was moderate. During the crop-growing seasons, specifically summer and spring, the relationship was relatively weaker. However, in the winter and autumn seasons, when the crop leaves reached maturity, the correlation between the LAI and LST was relatively stronger (Table 5).

Discussion

This study examined the temporal variations in LAI and LST by mapping the mean value of these two variables in the Millie watershed from 2016 to 2022 using Sentinel-2 LAI and Landsat 8/9 LST products. We investigated the temporal trends of mean LAI and LST in the study area
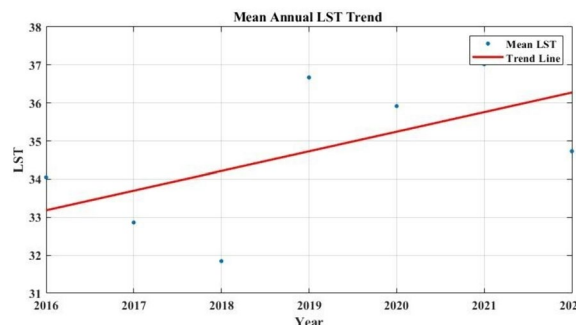
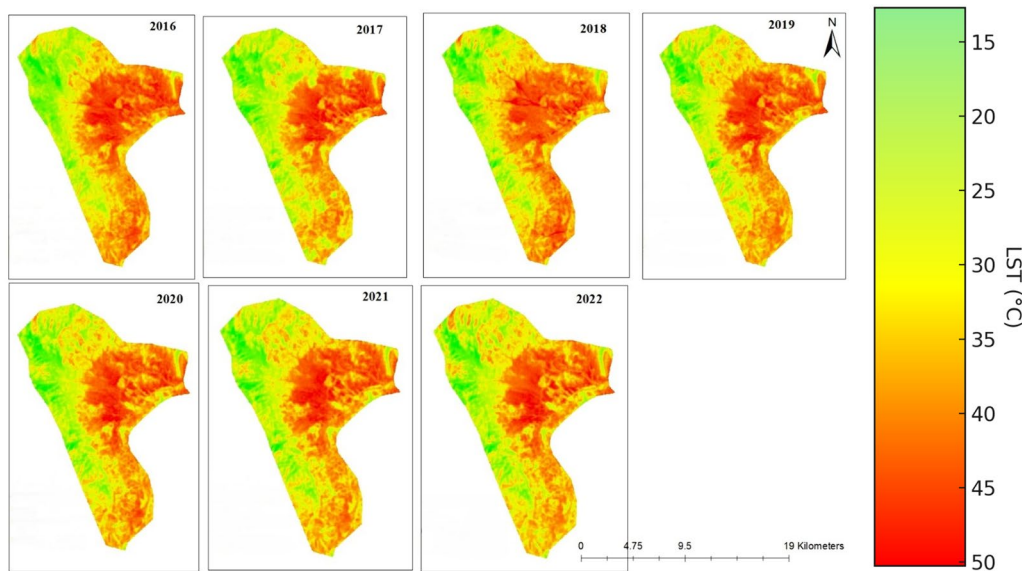**Fig. 8** Annual trend of mean LST from 2016 to 2022: an insignificant positive trend with a 0.466 Sen's slope

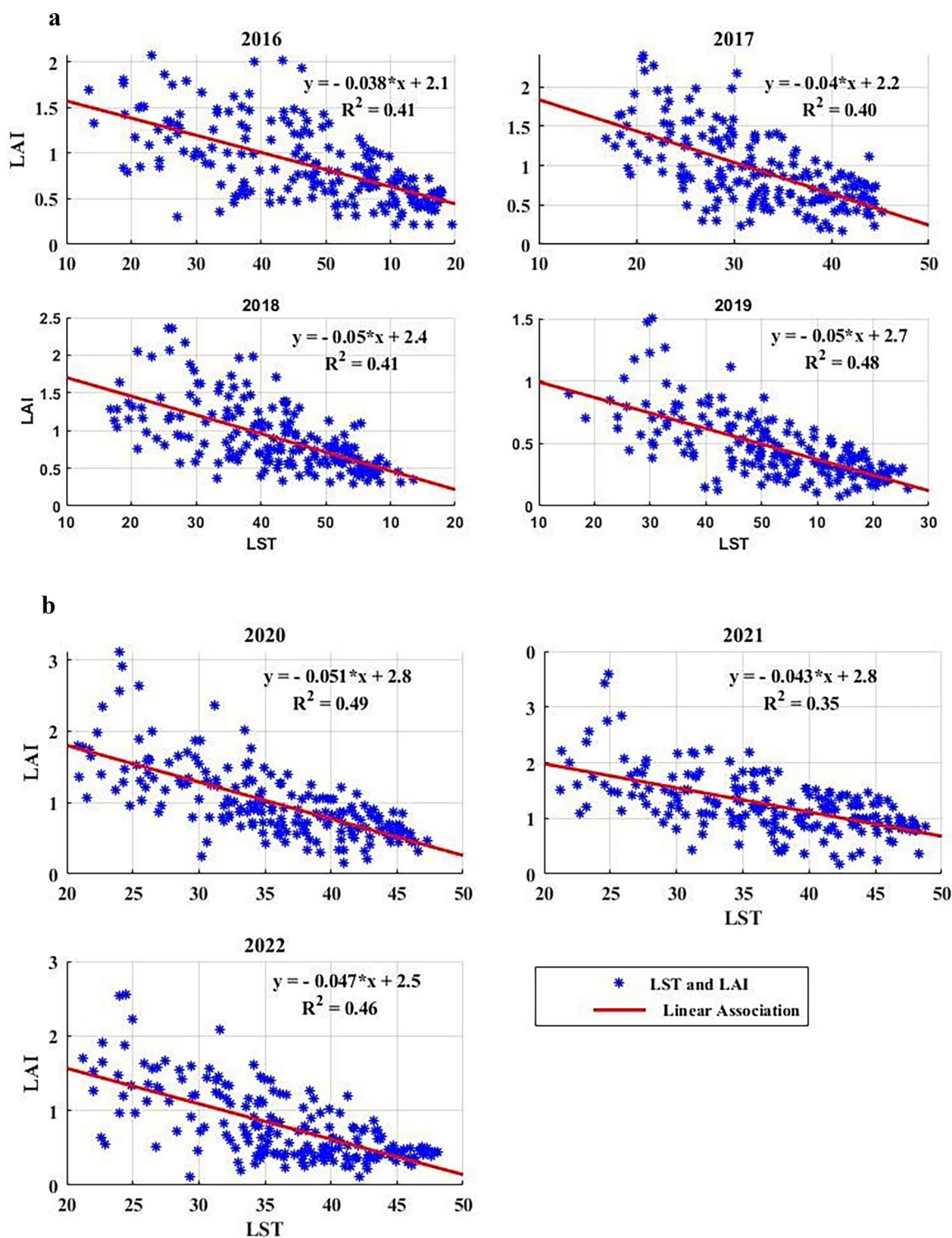**Fig. 7** Mean annual LST maps of the study area from 2016 to 2022

Ahmed *et al. Environmental Systems Research*   (2024) 13:43

Page 10 of 15

a

2016

$y = -0.038*x + 2.1$
$R^2 = 0.41$

2017

$y = -0.04*x + 2.2$
$R^2 = 0.40$

2018

$y = -0.05*x + 2.4$
$R^2 = 0.41$

2019

$y = -0.05*x + 2.7$
$R^2 = 0.48$

b

2020

$y = -0.051*x + 2.8$
$R^2 = 0.49$

2021

$y = -0.043*x + 2.8$
$R^2 = 0.35$

2022

$y = -0.047*x + 2.5$
$R^2 = 0.46$

* LST and LAI
— Linear Association

Fig. 9 **a** Annual association between LAI and LST from 2016 to 2019. **b** Annual association between LAI and LST from 2020 to 2022
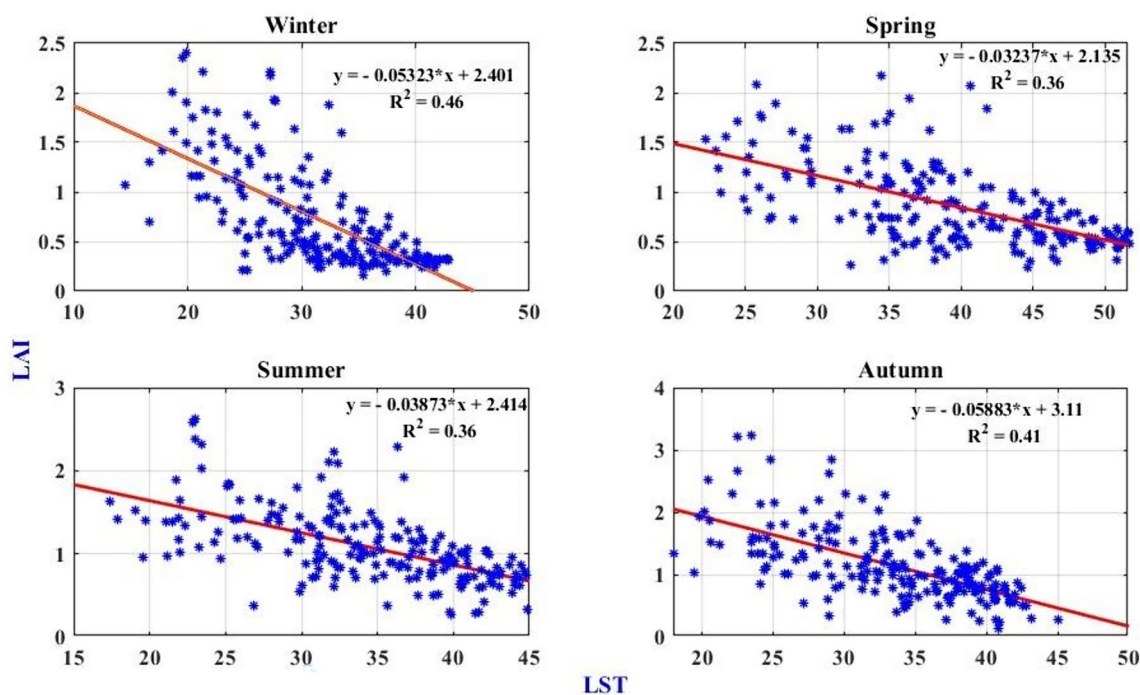
Fig. 10 Seasonal association between LAI and LST from 2016 to 2022

at both seasonal and annual scales. Our analysis indicated a generally significant increasing trend in the mean LAI during the study period, whereas the LST value exhibited an insignificant positive trend.

Seasonal and annual trends of LAI

Our findings revealed a significant greening trend in the Millie watershed from 2016 to 2022, with positive Sen's slope values observed in the winter, summer, and autumn seasons. These results are consistent with prior research indicating a global increase in the LAI during growing

Table 5 R^2, adjusted R^2 and P value of annual and seasonal correlation between LAI and LST

Seasons	R^2	Adjusted R^2	P Value <
2016	0.4119	0.4088	2.20E-16
2017	0.4012	0.3981	2.20E-16
2018	0.4104	0.4074	2.20E-16
2019	0.4763	0.4736	2.20E-16
2020	0.4934	0.4908	2.20E-16
2021	0.3452	0.3418	2.20E-16
2022	0.4594	0.4566	2.20E-16
Winter	0.4602	0.4575	2.20E-16
Spring	0.3580	0.3548	2.20E-16
Summer	0.3552	0.3520	2.20E-16
Autumn	0.4065	0.4036	2.20E-16

seasons (Rasul et al. 2020). This trend can be attributed to a combination of factors, including natural reforestation, improved land use management practices, and increased agricultural activity in the study area. However, the negative Sen's slope value observed during the spring season is attributed to a declining trend in spring rainfall, which results in reduced vegetation growth. This relationship is supported by Abegaz and Abera (2020), who examined temperature and rainfall trends in northeastern Ethiopia, specifically South Wollo, and found a declining rainfall trend in the spring.

The mean LAI value exhibited seasonal variation, ranging from 0.020 to 0.082 (Figs. 4 and 5). Nevertheless, the trendp (trend during the study period) was consistently robust, ranging from 0.137 to 0.576. These findings suggest that while short-term seasonal trends may exhibit some variability, the overall trend of increasing LAI throughout the study period remains substantial.

As reported by SuDCA and Soberland (2015) and Agri Service Ethiopia (ASE) in 2011), agriculture is the primary land use in the study area. Consequently, examining seasonal trends is crucial due to the varying spatial patterns of seasonal crops affected by factors like rainfall and temperature. Our findings solidify the close connection between the trend of LAI and agricultural activities. Seasons marked by abundant rainfall, accompanied by a gradual expansion of cultivated lands, have resulted in higher mean LAI trends.

Ahmed *et al. Environmental Systems Research*   (2024) 13:43

Page 12 of 15

According to Abegaz and Abera (2020), who investigated temperature and rainfall trends in northeastern Ethiopia, the seasonal rainfall trend in this region, particularly in South Wollo, has shown a declining trend in the spring season, relatively stable trends in summer and autumn, and an increasing trend in the winter season. A decreasing trend in spring season rainfall leads to less cultivation, which negatively impacts the LAI. Consequently, the declining trend of the mean LAI in the spring season is attributed to insufficient rainfall, which negatively impacts agricultural activities (Agidew and Singh 2017). The relative increase in the mean LAI during the winter season is attributed to increased rainfall, which positively influences rainfed agriculture (Chuanhua et al. 2023; Rasul et al. 2020). Hence, an increasing or decreasing trend in the LAI can be predicted based on rainfall availability, which directly impacts agricultural practices (Zhu et al. 2016). These results affirm the positive influence of rainfall amount on LAI (Longhui et al. 2017), as most of the greening trends were observed during the growing season.

Seasonal and annual trends of LST
Throughout the years 2016 to 2022, the average LST in the study area did not significantly change seasonally or annually, except for a notable trend observed during summer season with a 93% confidence level (Figs. 6 and 8). Abegaz and Abera (2020), a study in southern Wollo, Ethiopia, found that the delayed onset of the summer season, which initially results in sparse rainfall, leads to an increase in LST. Conversely, this delay causes increased rainfall at the end of summer and into the autumn, which enhances agricultural activity and contributes to a lower LST trend during the autumn season. Reduced rainfall and soil moisture positively impact LST through their effects on crop cultivation (Jiang et al. 2023; Sun and Pinker 2004; Weng et al. 2004). These findings support the notion that changes in rainfall amounts, soil moisture, and crop production inversely influence LSTs by modulating the transmission of electromagnetic radiation to the Earth's surface. Therefore, the distinct LST trend observed in the autumn season, compared to other seasons, is due to the unique climatic and agricultural conditions of this period. Our findings further support this conclusion, revealing the highest LAI trend occurring in autumn.

Moisa et al. (2022a) and Moisa et al. (2022b) utilized one-way trend analysis and reported increments of 5 ℃ and 5.6 ℃, respectively, in the mean LST within Ethiopian tropical regions. In contrast, when we applied the one-way trend analysis in our study area, we observed an increment of only 0.68 ℃ in LST. The higher LST increment in their studies can be attributed to a longer study period, whereas the lower increment in our study is due

to the shorter study period. Furthermore, in our study, the reported 3 ℃ increase over 7 years is based on Sen's slope, a more appropriate trend analysis method for time-series data. Sen's slope uses the median of all observed data, providing a robust estimate of the trend. This method can result in a higher apparent rate of increase because it accounts for all data points rather than just the initial and final year mean LST values.

The studies conducted by Moisa et al. (2022a) and (Moisa et al. 2022b) in similar climatic environments within Ethiopia offer valuable insights that support our findings. Their study area and the observed increments in LST can be cross-referenced with our data, strengthening the validity of our results. The robust estimation provided by Sen's slope in our study underscores the necessity of using comprehensive analysis methods to capture the nuanced impacts of climatic variations on LST. Additionally, the observed LST trends in both studies align with the broader understanding of how seasonal shifts and agricultural activities influence surface temperatures, reaffirming the intricate relationship between environmental factors and LST dynamics in tropical regions.

Seasonal and annual association between LAI and LST
The relationship between mean LAI and LST was evaluated yearly to understand how vegetation responds to variations in surface temperature, as depicted in Fig. 9a, b. Our analysis revealed a moderate inverse correlation between the mean LAI and LST from 2016 to 2022, with the R^2 ranging from 0.35 to 0.49. This finding contrasts with the results of Rasul et al. (2020), who found no significant relationship between LAI and LST in Africa. However, it aligns with the findings of Guha and Govil (2020), who reported a moderate correlation between NDVI and LST in the tropical region of India. The moderate negative correlation observed in this study suggested that photosynthetic vegetation in the study area is sensitive to LST. Variations in vegetation type, land use practices, and local climatic conditions contributed to the observed moderate correlations (Guha and Govil 2020). Different vegetation types have unique characteristics and responses to temperature changes, influencing the overall LST in diverse ways. Additionally, agricultural activities, deforestation, and urbanization can alter the land surface properties (Jaafar et al. 2020; Zhang et al. 2005), thereby impacting the LST. Furthermore, local climatic conditions, including temperature, precipitation, and humidity, further influence the relationship between these two variables (Yu et al. 2020). Regions with higher rainfall and cooler temperatures show stronger correlations between LAI and LST due to the enhanced growth of vegetation, while arid regions might display weaker correlations due to limited vegetation cover.

The seasonal correlation analysis between LAI and LST in the Mille watershed presented a complex relationship, with the strongest correlation occurring during the winter season ($R^2 = 0.46$) and the weakest during the spring and summer ($R^2 = 0.36$). This pattern suggests that vegetation's response to surface temperature is more pronounced when crops are mature, as seen in the stronger correlations during the winter and autumn seasons. These seasons coincide with crop maturity, indicating that mature vegetation has a greater influence on LST, potentially due to increased canopy cover and evapotranspiration rates, which contribute to cooling the surface.

Conversely, the correlation was weaker during the crop-growing seasons of summer and spring. While these seasons are marked by an increased mean LAI, the relationship between LAI and LST was less robust. This can be attributed to the higher temperatures and moderate rainfall from March to June, which drive intensive leaf development. During this period, the growing vegetation contributes to a cooling effect on LST, but the rapid changes in temperature and precipitation may also introduce variability, reducing the overall correlation.

Moreover, the study underscores the importance of considering various factors such as crop cultivation cycles, precipitation availability, land use practices, and mean maximum temperature in understanding the seasonal dynamics of the LAI-LST relationship. The lower R^2 values observed during the colder months, when crop cultivation is less optimal, further emphasize how these environmental and agricultural variables modulate the interaction between vegetation and surface temperature. This deeper understanding of seasonal variations is crucial for accurately modelling and predicting the impacts of climate and land use changes on vegetation dynamics in tropical regions.

Conclusion

This study highlighted a significant greening trend over the study period attributed to natural reforestation, land-use changes, and agricultural activities. While the LST showed relatively stable patterns, an increase during delayed summer onset was noted. The moderate inverse correlation between LAI and LST underscores vegetation sensitivity to temperature changes, emphasizing the need for vigilant environmental monitoring and management. These findings stress the importance of understanding the complex interplay between environmental factors, guiding the development of targeted strategies for sustainable land management and conservation in the region. While this study provides valuable insights into the temporal trends and correlation between LAI and LST in the Millie watershed, further research is needed to better understand the complex relationships between environmental factors and vegetation productivity in a broader context. To provide a more comprehensive understanding of the relationship between LAI and LST across different environments, future research should incorporate longer study periods and encompass a variety of climatic zones.

Availability of data and materials
The datasets used and/or analyzed during the current study are available from the corresponding author upon reasonable request.

Declarations

Ethics approval and consent to participate
Not applicable.

Consent for publication
Not applicable.

Competing interests
The authors declare that they have no competing interests.

References
Abegaz WB, Abera EA (2020) Temperature and rainfall trends in North Eastern Ethiopia. Clim WeatherForecasting. https://doi.org/10.35248/2332-2594.2020.8.262

Agidew A, Singh KN (2017) The implications of land use and land cover changes for rural household food insecurity in the Northeastern highlands of Ethiopia: the case of the Teleyayen sub - watershed. Agric Food Secur. https://doi.org/10.1186/s40066-017-0134-4

Agri Service Ethiopia (ASE). 2011. agri-drum-july-september-update.pdf.

Avdan, U, Jovanovska G (2016) Algorithm for automated mapping of land surface temperature using LANDSAT 8 satellite data.Journal of Sensors. https://doi.org/10.1155/2016/1480307

Baldocchi DD, Wilson KB, Gu L (2002) How the environment, canopy structure and canopy physiological functioning influence carbon, water and energy fluxes of a temperate broad-leaved deciduous forest - an assessment with the biophysical model CANOAK. Tree Physiol 22(15–16):1065–1077. https://doi.org/10.1093/treephys/22.15-16.1065

Berger K, Atzberger C, Danner M, D'Urso G, Mauser W, Vuolo F, Hank T (2018) Evaluation of the PROSAIL model capabilities for future hyperspectral model environments: a review study. Remote Sens. https://doi.org/10.3390/rs10010085

Birhanu L, Bekele T, Tesfaw B, Demissew S (2021) Relationships between topographic factors, soil and plant communities in a dry afromontane forest

Ahmed *et al. Environmental Systems Research*   (2024) 13:43

Page 14 of 15

patches of Northwestern Ethiopia. PLoS ONE 16:1–18. https://doi.org/10.1371/journal.pone.0247966

Blain GC (2013) Teste de Mann-Kendall: a necessidade de considerar a interação entre correlação serial e tendência. Acta Scientiarum Agron 35(4):393–402. https://doi.org/10.4025/actasciagron.v35i4.16006

Cheruy F, Dufresne JL, Aït Mesbah S, Grandpeix JY, Wang F (2017) Role of soil thermal inertia in surface temperature and soil moisture-temperature feedback. J Adv Model Earth Syst 9(8):2906–2919. https://doi.org/10.1002/2017MS001036

Chuanhua L, Li L, Wu X, Tsunekawa A, Wei Y, Liu Y, Peng L, Chen J, Bai K (2023) Increasing precipitation promoted vegetation growth in the Mongolian Plateau during 2001–2018. Front Environ Sci 11(May):1–15. https://doi.org/10.3389/fenvs.2023.1153601

Clevers JGPW, Kooistra L, van Brande Marnix MM (2017) Using Sentinel-2 data for retrieving LAI and leaf and canopy chlorophyll content of a potato crop. Remote Sens 9(5):1–15. https://doi.org/10.3390/rs9050405

Crawford CJ, Roy DP, Arab S, Barnes C, Vermote E, Hulley G, Gerace A, Choate M, Engebretson C, Micijevic E, Schmidt G, Anderson C, Anderson M, Bouchard M, Cook B, Dittmeier R, Howard D, Jenkerson C, Kim M, Zahn S (2023) The 50-year landsat collection 2 archive. Sci Remote Sens 8:100103. https://doi.org/10.1016/j.srs.2023.100103

Desalegn MY, Miheretu BA, Gobezie T (2023) Impact of land use/land cover changes on soil erosion risk in upper Mile River sub-watershed, North Eastern highlands of Ethiopia. Geol Ecol Landsc 00(00):1–13. https://doi.org/10.1080/24749508.2023.2206063

Destaw F (2017) Rainfall and temperature trend analysis at indibir station. Int J Environ Monit Anal 11(3):63–71. https://doi.org/10.11648/j.ijema.20231103.12

Fashing PJ, Nguyen N, Demissew S, Gizaw A, Atickem A, Mekonnen A, Nurmi NO, Kerby J.T, Stenseth NC (2022) Ecology, evolution, and conservation of Ethiopia's biodiversity. Proc Natl Acad Sci. https://doi.org/10.1073/pnas.2206635119

Guechi I, Gherraz H, Alkama D (2021) Correlation analysis between biophysical indices and land surface temperature using remote sensing and GIS in Guelma city (Algeria). Bulletin de La Societe Royale Des Sciences de Liege 90:158–180. https://doi.org/10.25518/0037-9565.10457

Guha S, Govil H (2020) Land surface temperature and normalized difference vegetation index relationship: a seasonal study on a tropical city. SN Appl Sci 2(10):1–14. https://doi.org/10.1007/s42452-020-03458-8

Hamed KH (2008) Trend detection in hydrologic data: the Mann-Kendall trend test under the scaling hypothesis. J Hydrol 349(3–4):350–363. https://doi.org/10.1016/j.jhydrol.2007.11.009

Han G, Wang J, Pan Y, Huang N, Zhang Z, Peng R, Wang Z, Sun G, Liu C, Ma S, Song Y, Pan Z (2020) Temporal and spatial variation of soil moisture and its possible impact on regional air temperature in China. Water. https://doi.org/10.3390/w12061807

Han D, Liu J, Zhang R, Liu Z, Guo T, Jiang H, Wang J, Zhao H, Ren S, Yang P (2023) Evaluation of the SAIL radiative transfer model for simulating canopy reflectance of row crop canopies. Remote Sens. https://doi.org/10.3390/rs15235433

Haylemariyam MB (2018) Detection of land surface temperature in relation to land use land cover change: Dire Dawa City, Ethiopia. J Remote Sens GIS. https://doi.org/10.4172/2469-4134.1000245

Hussain S, Raza A, Abdo HG, Mubeen M, Tariq A, Nasim W, Majeed M, Almohamad H, Al Dughairi AA (2023) Relation of land surface temperature with different vegetation indices using multi-temporal remote sensing data in Sahiwal region, Pakistan. Geosci Lett. https://doi.org/10.1186/s40562-023-00287-6

Imran HM, Hossain A, Islam AKMS, Rahman A, Bhuiyan MAE, Paul S, Alam A (2021) Impact of land cover changes on land surface temperature and human thermal comfort in Dhaka City of Bangladesh. Earth Syst Environ 5(3):667–693. https://doi.org/10.1007/s41748-021-00243-4

Jacquemoud S, Ustin SL, Verdebout J, Schmuck G, Andreoli G, Hosgood B (1996) Estimating leaf biochemistry using the PROSPECT leaf optical properties model. Remote Sens Environ 56(3):194–202. https://doi.org/10.1016/0034-4257(95)00238-3

Jacquemoud S, Verhoef W, Baret F, Bacour C, Zarco-Tejada PJ, Asner GP, François C, Ustin SL (2009) PROSPECT + SAIL models: a review of use for vegetation characterization. Remote Sens Environ 113(SUPPL. 1):S56–S66. https://doi.org/10.1016/j.rse.2008.01.026

Jiang J, Comar A, Burger P, Bancal P, Weiss M, Baret F (2018) Estimation of leaf traits from reflectance measurements : comparison between methods based on vegetation indices and several versions of the PROSPECT model. Plant Methods. https://doi.org/10.1186/s13007-018-0291-x

Jiang K, Pan Z, Pan F, Teuling AJ, Han G, An P, Chen X, Wang J, Song Y, Cheng L, Zhang Z, Huang N, Ma S, Gao R, Zhang Z, Men J, Lv X, Dong Z (2023) Combined influence of soil moisture and atmospheric humidity on land surface temperature under different climatic background. Iscience 26(6):106837. https://doi.org/10.1016/j.isci.2023.106837

Jin M, Zhang DL (2002) Observed variations of leaf area index and its relationship with surface temperatures during warm seasons. Meteorol Atmos Phys 80(1–4):117–129. https://doi.org/10.1007/s007030200019

Kamenova I, Dimitrov P (2021) Evaluation of Sentinel-2 vegetation indices for prediction of LAI, fAPAR and fCover of winter wheat in Bulgaria. Europ J Remote Sens 54(sup1):89–108. https://doi.org/10.1080/22797254.2020.1839359

Kganyago M, Mhangara P, Alexandridis T, Laneve G, Ovakoglou G, Mashiyi N (2020) Validation of sentinel-2 leaf area index (LAI) product derived from SNAP toolbox and its comparison with global LAI products in an African semi-arid agricultural landscape. Remote Sens Lett 11(10):883–892. https://doi.org/10.1080/2150704X.2020.1767823

Kume A (2017) Importance of the green color, absorption gradient, and spectral absorption of chloroplasts for the radiative energy balance of leaves. J Plant Res 130(3):501–514. https://doi.org/10.1007/s10265-017-0910-z

Li ZL, Tang BH, Wu H, Ren H, Yan G, Wan Z, Trigo IF, Sobrino JA (2013) Satellite-derived land surface temperature: current status and perspectives. Remote Sens Environ 131:14–37. https://doi.org/10.1016/j.rse.2012.12.008

Li W, Migliavacca M, Forkel M, Denissen JMC, Reichstein M, Yang H, Duveiller G, Weber U, Orth R (2022) Widespread increasing vegetation sensitivity to soil moisture. Nat Commun 13(1):1–9. https://doi.org/10.1038/s41467-022-31667-9

Liu L, Zhang R, Zuo Z (2016) The relationship between soil moisture and LAI in different types of soil in central eastern China. J Hydrometeorol 17(11):2733–2742. https://doi.org/10.1175/JHM-D-15-0240.1

Longhui L, Wang YP, Beringer J, Shi H, Cleverly J, Cheng L, Eamus D, Huete A, Hutley L, Lu X, Piao S, Zhang L, Zhang Y, Yu Q (2017) Responses of LAI to rainfall explain contrasting sensitivities to carbon uptake between forest and non-forest ecosystems in Australia. Sci Rep 7(1):1–9. https://doi.org/10.1038/s41598-017-11063-w

Miller DL, Alonzo M, Meerdink SK, Allen MA, Tague CL, Roberts DA, McFadden JP (2022) Seasonal and interannual drought responses of vegetation in a California urbanized area measured using complementary remote sensing indices. ISPRS J Photogramm Remote Sens 183:178–195. https://doi.org/10.1016/j.isprsjprs.2021.11.002

Mohd Jaafar WSW, Maulud KNA, Muhmad Kamarulzaman AM, Raihan A, Sah SM, Ahmad A, Maizah Saad SN, Mohd Azmi AT, Syukri NKAJ, Khan WR (2020) The influence of deforestation on land surface temperature-a case study of Perak and Kedah, Malaysia. Forests. https://doi.org/10.3390/F11060670

Moisa MB, Dejene IN, Merga BB, Gemeda DO (2022a) Impacts of land use/land cover dynamics on land surface temperature using geospatial techniques in Anger River Sub-basin, Western Ethiopia. Environ Earth Sci 81(3):1–14. https://doi.org/10.1007/s12665-022-10221-2

Moisa MB, Gabissa BT, Hinkosa LB, Dejene IN, Gemeda DO (2022b) Analysis of land surface temperature using Geospatial technologies in Gida Kiremu, Limu, and Amuru District, Western Ethiopia. Artif Intell Agric 6:90–99. https://doi.org/10.1016/j.aiia.2022.06.002

Moravec D, Komárek J, Medina SLC, Molina I (2021) Effect of atmospheric corrections on NDVI: Intercomparability of Landsat 8, Sentinel-2, and UAV sensors. Remote Sens 13(18):1–14. https://doi.org/10.3390/rs13183550

Mourad R, Jaafar H, Anderson M, Gao F (2020) Assessment of leaf area index models using harmonized Landsat and Sentinel-2 surface reflectance data over a semi-arid irrigated landscape. Remote Sens. https://doi.org/10.3390/RS12193121

Muir C, Southworth J, Khatami R, Herrero H, Akyapı B (2021) Vegetation dynamics and climatological drivers in ethiopia at the turn of the century. Remote Sens 13(16):1–15. https://doi.org/10.3390/rs13163267

Mustafa EK, Liu G, Hassan A, Damos MA, Tarawally M (2020) Predicting of land surface temperature distribution in Freetown City, Sierra Leone by using polynomial curve fitting model. J Geogr Inform Syst. https://doi.org/10.4236/jgis.2020.125031

Ahmed *et al. Environmental Systems Research*   (2024) 13:43

Page 15 of 15

Mwangi PW, Karanja FN, Kamau PK (2018) Analysis of the relationship between land surface temperature and vegetation and built-up indices in Upper-Hill, Nairobi. J Geosci Environ Prot 06(01):1–16. https://doi.org/10.4236/gep.2018.61001

Myneni RB (1997) Estimation of global leaf area index and absorbed par using radiative transfer models. IEEE Trans Geosci Remote Sens 35(6):1380–1393. https://doi.org/10.1109/36.649788

Nega W, Hailu BT, Fetene A (2019) An assessment of the vegetation cover change impact on rainfall and land surface temperature using remote sensing in a subtropical climate, Ethiopia. Remote Sens Appl Soc Environ 16(August):100266. https://doi.org/10.1016/j.rsase.2019.100266

Pan N, Feng X, Fu B, Wang S, Ji F, Pan S (2018) Increasing global vegetation browning hidden in overall vegetation greening: Insights from time-varying trends. Remote Sens Environ 214(May):59–72. https://doi.org/10.1016/j.rse.2018.05.018

Park T, Chen C, Wang X, Piao S, Xu B, Chaturvedi RK, Fuchs R, Brovkin V, Ciais P, Fensholt R, Tømmervik H, Bala G, Zhu Z, Nemani RR, Myneni RB (2019) China and India lead in greening of the world through land-use management. Nat Sustain 2(2):122–129. https://doi.org/10.1038/s41893-019-0220-7

Rasul A, Ibrahim S, Onojeghuo AR, Balzter H (2020) A trend analysis of leaf area index and land surface temperature and their relationship from global to local scale. Land 9(10):1–17. https://doi.org/10.3390/land9100388

Reygadas Y, Jensen JLR, Moisen GG, Currit N, Chow ET (2020) Assessing the relationship between vegetation greenness and surface temperature through granger causality and impulse-response coefficients: a case study in Mexico. Int J Remote Sens 41(10):3761–3783. https://doi.org/10.1080/01431161.2019.1711241

Sayler K. Landsat 8–9 Level 2 Science Product (L2SP) Guide March 2022 Landsat. 2022; 8–9 (4.0, Vol. 2, Issue March).

Sayler K, LSRD Project Manager, U.S. Geological Survey. Landsat 8–9 Level 2 Science Product (L2SP) Guide. In Department of the Interior U.S. Geological Survey: Vol. Version 5. (Issue March). Survey, Department of the Interior U.S. Geological. 2023.

Schwaab J, Meier R, Mussetti G, Seneviratne S, Bürgi C, Davin EL (2021) The role of urban trees in reducing land surface temperatures in European cities. Nat Commun 12(1):1–11. https://doi.org/10.1038/s41467-021-26768-w

Seneshaw Getahun Y (2015) Analysis of climate variability (ENSO) and vegetation dynamics in Gojjam, Ethiopia. J Earth Sci Clim Change. https://doi.org/10.4172/2157-7617.1000320

Sharma AR, Badarinath KVS, Roy PS (2009) Comparison of ground reflectance measurement with satellite derived atmospherically corrected reflectance: a case study over semi-arid landscape. Adv Space Res 43(1):56–64. https://doi.org/10.1016/j.asr.2008.10.010

Skidmore A, Bijker W, Schmidt K, Kumar L (1997) Use of remote sensing and GIS for sustainable land management. ITC J 1997(3–4):302–315

Skidmore A (2002) Environmental Modelling with GIS and Remote Sensing (1st Ed.). Routledge.https://doi.org/10.4324/9780203302217. Accessed at https://ndl.ethernet.edu.et/bitstream/123456789/50182/1/1.pdf. Accesed15 Mar 2023

Sola I, García-Martín A, Sandonís-Pozo L, Álvarez-Mozos J, Pérez-Cabello F, González-Audícana M, Montorio Llovería R (2018) Assessment of atmospheric correction methods for Sentinel-2 images in Mediterranean landscapes. Int J Appl Earth Obs Geoinf 73(February):63–76. https://doi.org/10.1016/j.jag.2018.05.020

SuDCA, Soberland (2015) Assessment Report on Productive Safety Net Program (PSNP)- Public Works Impact Assessment; The Federal Democratic Republic of Ethiopia. October.

Sun D, Pinker RT (2004) Case study of soil moisture effect on land surface temperature retrieval. IEEE Geosci Remote Sens Lett 1(2):127–130. https://doi.org/10.1109/LGRS.2004.824749

Tesemma ZK, Wei Y, Peel MC, Western AW (2015) Including the dynamic relationship between climatic variables and leaf area index in a hydrological model to improve streamflow prediction under a changing climate. Hydrol Earth Syst Sci 19(6):2821–2836. https://doi.org/10.5194/hess-19-2821-2015

Wachmann A, Starko S, Neufeld CJ, Costa M (2024) Validating landsat analysis ready data for nearshore sea surface temperature monitoring in the Northeast Pacific. Remote Sens. https://doi.org/10.3390/rs16050920

Wang Y, Gastellu-Etchegorry JP (2020) DART: Improvement of thermal infrared radiative transfer modelling for simulating top of atmosphere radiance.

Remote Sens Environ 251(August):112082. https://doi.org/10.1016/j.rse.2020.112082

Wang XL, Swail V (2001) Changes in extreme wave heights in northern hemisphere oceans and related atmospheric circulation regimes. J Clim 14:2204. https://doi.org/10.1175/1520-0442(2001)014<2204:COEWHI>2.0.CO;2

Wang J, Xiao X, Bajgain R, Starks P, Steiner J, Doughty RB, Chang Q (2019) Estimating leaf area index and aboveground biomass of grazing pastures using Sentinel-1, Sentinel-2 and Landsat images. ISPRS J Photogramm Remote Sens 154:189–201. https://doi.org/10.1016/j.isprsjprs.2019.06.007

Wang F, Shao W, Yu H, Kan G, He X, Zhang D, Ren M, Wang G (2020) Re-evaluation of the power of the Mann-Kendall test for detecting monotonic trends in hydrometeorological time series. Front Earth Sci 8(February):1–12. https://doi.org/10.3389/feart.2020.00014

Weiss M, Baret F (2016) S2ToolBox Level 2 products: LAI, FAPAR, FCOVER - Version 1.1. ed. Institut National de la Recherche Agronomique, Avignon, France. http://step.esa.int/docs/extra/ATBD_S2ToolBox_L2B_V1.1.pdf. Accessed 15 Mar 2023

Weng Q, Lu D, Schubring J (2004) Estimation of land surface temperature-vegetation abundance relationship for urban heat island studies. Remote Sens Environ 89(4):467–483. https://doi.org/10.1016/j.rse.2003.11.005

Woodcock CE, Strahler AH, Franklin J (1983) Remote sensing for land management and planning. Environ Manag. 7:223–237. https://doi.org/10.1007/BF01871537

Worku MA, Feyisa GL, Beketie KT, Garbolino E (2023) Spatiotemporal dynamics of vegetation in response to climate variability in the Borana rangelands of southern Ethiopia. Front Earth Sci 11(January):1–15. https://doi.org/10.3389/feart.2023.991176

Xie Q, Dash J, Huete A, Jiang A, Yin G, Ding Y, Peng D, Hall CC, Brown L, Shi Y, Ye H, Dong Y, Huang W (2019) Retrieval of crop biophysical parameters from Sentinel-2 remote sensing imagery. Int J Appl Earth Obs Geoinf 80(April):187–195. https://doi.org/10.1016/j.jag.2019.04.019

Yeneneh N, Elias E, Feyisa GL (2022) Detection of land use/land cover and land surface temperature change in the Suha Watershed, North-Western Highlands of Ethiopia. Environ Chall 7(April):100523. https://doi.org/10.1016/j.envc.2022.100523

Yu L, Liu Y, Liu T, Yan F (2020) Impact of recent vegetation greening on temperature and precipitation over China. Agric for Meteorol 295(September):108197. https://doi.org/10.1016/j.agrformet.2020.108197

Yue S, Wang CY (2004) The Mann-Kendall test modified by effective sample size to detect trend in serially correlated hydrological series. Water Resour Manage 18(3):201–218. https://doi.org/10.1023/B:WARM.0000043140.61082.60

Yue S, Pilon P, Cavadias G, Phinney B (2002) The influence of autocorrelation on the ability to detect trend in hydrological series. Hydrol Process. https://doi.org/10.1002/hyp.1095

Zhang J, Dong W, Wu L, Wei J, Chen P, Lee DK (2005) Impact of land use changes on surface warming in China. Adv Atmos Sci 22(3):343–348. https://doi.org/10.1007/bf02918748

Zhu Z, Piao S, Myneni RB, Huang M, Zeng Z, Canadell JG, Ciais P, Sitch S (2016) Greening of the Earth and its drivers. Nat Clim Change. https://doi.org/10.1038/nclimate3004

Publisher's Note